Article

Magnetooptics in Cylindrical Structures

Štefan Višňovský[iD]

Faculty of Mathematics and Physics, Charles University, Prague, Czech Republic; visnov@karlov.mff.cuni.cz

Abstract: Understanding magnetooptics in cylindrical structures presents interest in the development of magnetic sensor and nonreciprocal devices compatible with optical fibers. The present work studies wave propagation in dielectric circular cylindrical structures characterized by magnetic permeability and electric permittivity tensors at axial magnetization. The Helmholtz equations deduced from the Maxwell equations in transverse circularly polarized representation provide electric and magnetic fields. With the restriction to terms linear in off-diagonal tensor elements, these can be expressed analytically. The results are applied to magnetooptic (MO) circular cylindrical waveguides with a step refractive index profile. The nonreciprocal propagation is illustrated on waveguides with an yttrium iron garnet (YIG) core and a lower refractive index cladding formed by gallium substituted yttrium iron garnet (GaYIG) at the optical communication wavelength. The propagation distance required for the isolator operation is about one hundred micrometers. The approach may be applied to other structures of cylindrical symmetry in the range from microwave to optical frequencies.

Keywords: magnetooptical effect; Faraday effect; nonreciprocity; isolator

1. Introduction

Electromagnetic waves in magnetized media depend on magnetization and often show nonreciprocal propagation. The phenomenon is exploited in sensors and devices such as waveguide isolators, phase shifters, circulators, and modulators. Their operation can be explained by considering circularly polarized (CP) transverse electromagnetic waves of opposite handedness ($\pm$) propagating in infinite lossless uniformly magnetized media. In such media, the propagation vectors, $\mathbf{k}_{\pm}$, slightly differ in magnitude and are both oriented parallel to the medium magnetization $\mathbf{M}$, i.e., $\mathbf{k} \| \mathbf{M}$. Then the CP waves represent eigenmodes, one pair in forward direction and another one in reversed direction [1].

At oblique wave incidence in perpendicularly magnetized multilayers or in planar, cylindrical or channel waveguides with axial $\mathbf{M}$, the eigenmodes are no more CP waves [2–7]. In circular cylindrical waveguides, the eigenmodes can only be approximated by decoupled CP waves, particularly in the weak guidance limit [8–13]. The analysis of magnetic waveguide structures is often complex and, in most cases, requires numerical methods [14–16]. In the microwave region, the effect of $\mathbf{M}$ is deduced from the tensor nature of magnetic permeability with the scalar electric permittivity [17] while in the near infrared and visible regions, the analysis assumes the tensor nature of electric permittivity with magnetic permeability reduced to its vacuum value [18,19]. In both cases, the diagonal and off-diagonal tensor elements are even and odd functions of $\mathbf{M}$, respectively [18–23]. In the infrared and visible spectral regions, a more rigorous treatment would account for the tensorial nature of both material parameters [24–29].

The present work provides an analytical approach to the problems of circular cylindrical structures displaying magnetooptic (MO) activity induced by axial magnetization. The approach covers the frequency range from microwave to optical frequencies. The i-th medium in a cylindrically layered structure is characterized by the magnetic permeability, $\tilde{\mu}^{(i)}$, and electric permittivity, $\tilde{\varepsilon}^{(i)}$, tensors

for axial $\mathbf{M}^{(i)}$. The work represents an extension of a previous study on the Helmholtz equation in isotropic cylindrical structures [30]. The final expressions provide insight into the trends and the symmetry which are difficult to appreciate in the use of numerical methods. To the best of the author's knowledge, the problem was not treated before with the exception of a previous study on the Faraday effect in optical fibers characterized by the gyroelectric dielectric permittivity tensors published by Yoshino [12]. The study assumed CP eigenmodes, an approximation justified to some extent only in the weak guiding limit.

The presentation is organized into five sections. The Helmholtz vector wave equations deduced from the Maxwell equations in transverse circularly polarized (TCP) representation provide electric, $\mathbf{E}^{(i)}$, and magnetic, $\mathbf{H}^{(i)}$, fields (Sections 2 and 3). With the restriction to terms linear in the off-diagonal elements of $\tilde{\varepsilon}^{(i)}$ and $\tilde{\mu}^{(i)}$, these can be expressed analytically as functions of circular cylindrical coordinates ϱ, φ, and z. The analysis results are applied to the simplest cylindrically layered structure, an optical fiber with step refractive index profile, formed by a uniform core and a uniform cladding. The conditions for waveguiding in the structure follow from the boundary conditions for $\mathbf{E}^{(i)}$ and $\mathbf{H}^{(i)}$ at the core—cladding interface. These provide eigenvalue equations for pairs of longitudinal propagation constants, $\beta_{\pm}$. The difference $\beta_+ - \beta_-$ characterizes the nonreciprocity. The nonreciprocal propagation is illustrated on waveguides with yttrium iron garnet ($Y_3Fe_3O_{12}$) core and lower refractive index cladding formed by gallium substituted yttrium iron garnet ($Y_3Fe_{5-x}Ga_xO_{12}$) at the optical communication wavelength of 1.55 µm (Section 4). The conclusions are briefly summarized in Section 5.

2. Maxwell Equations

For the time, t, dependence of harmonic waves propagating with the angular frequency, ω, and described by a factor $\exp(j\omega t)$, the Maxwell equations in a linear medium (i) characterized by the electric permittivity tensor, $\tilde{\varepsilon}^{(i)}$, and magnetic permeability tensor, $\tilde{\mu}^{(i)}$, become

$$\nabla \times \mathbf{E}^{(i)} = -j\omega\tilde{\mu}^{(i)}\mathbf{H}^{(i)}, \tag{1a}$$

$$\nabla \times \mathbf{H}^{(i)} = j\omega\tilde{\varepsilon}^{(i)}\mathbf{E}, \tag{1b}$$

$$\nabla \cdot \left(\tilde{\varepsilon}^{(i)}\mathbf{E}^{(i)} \right) = 0, \tag{1c}$$

$$\nabla \cdot \left(\tilde{\mu}^{(i)}\mathbf{H}^{(i)} \right) = 0. \tag{1d}$$

A linear homogeneous originally isotropic region (i) magnetically ordered parallel to the z-axis of a Cartesian coordinate system is characterized by the electric permittivity tensor

$$\tilde{\varepsilon}^{(i)} = \begin{pmatrix} \varepsilon_0^{(i)} & -j\varepsilon_1^{(i)} & 0 \\ j\varepsilon_1^{(i)} & \varepsilon_0^{(i)} & 0 \\ 0 & 0 & \varepsilon_z^{(i)} \end{pmatrix} \tag{2a}$$

and by the magnetic permeability tensor

$$\tilde{\mu}^{(i)} = \begin{pmatrix} \mu_0^{(i)} & -j\mu_1^{(i)} & 0 \\ j\mu_1^{(i)} & \mu_0^{(i)} & 0 \\ 0 & 0 & \mu_z^{(i)} \end{pmatrix} \tag{2b}$$

For the electric and magnetic wave field vectors in TCP representation, where $E_{\pm}^{(i)} = E_{\pm}^{(i)}(\varrho, \varphi, z)$ and $H_{\pm}^{(i)} = H_{\pm}^{(i)}(\varrho, \varphi, z)$, $E_z^{(i)} = E_z^{(i)}(\varrho, \varphi, z)$ and $H_z^{(i)} = H_z^{(i)}(\varrho, \varphi, z)$,

$$\mathbf{E}^{(i)}\left(\varrho,\varphi,z,t\right) = \left(\mathrm{e}^{-\mathrm{j}\varphi}\hat{\varrho}_{+}E_{+}^{(i)} + \mathrm{e}^{\mathrm{j}\varphi}\hat{\varrho}_{-}E_{-}^{(i)} + E_{z}^{(i)}\hat{z}\right)\exp\left(\mathrm{j}\omega t\right), \tag{3a}$$

$$\mathbf{H}^{(i)}\left(\varrho,\varphi,z,t\right) = \left(\mathrm{e}^{-\mathrm{j}\varphi}\hat{\varrho}_{+}H_{+}^{(i)} + \mathrm{e}^{\mathrm{j}\varphi}\hat{\varrho}_{-}H_{-}^{(i)} + H_{z}^{(i)}\hat{z}\right)\exp\left(\mathrm{j}\omega t\right), \tag{3b}$$

the Maxwell curl equations in the transverse ($\hat{\varrho}_{\pm}$) and axial ($\hat{z}$) components are given by

$$
\begin{aligned}
&\hat{\varrho}_{+}\mathrm{e}^{-\mathrm{j}\varphi}\left[-\frac{\partial E_{+}^{(i)}}{\partial z} + 2^{-1/2}\left(\frac{\partial}{\partial\varrho} - \mathrm{j}\frac{1}{\varrho}\frac{\partial}{\partial\varphi}\right)E_{z}^{(i)}\right] + \hat{\varrho}_{-}\mathrm{e}^{\mathrm{j}\varphi}\left[\frac{\partial E_{-}^{(i)}}{\partial z} - 2^{-1/2}\left(\frac{\partial}{\partial\varrho} + \mathrm{j}\frac{1}{\varrho}\frac{\partial}{\partial\varphi}\right)E_{z}^{(i)}\right] \\
&+\; 2^{-1/2}\hat{z}\left[\frac{1}{\varrho}E_{+}^{(i)} + \left(\frac{\partial}{\partial\varrho} + \mathrm{j}\frac{1}{\varrho}\frac{\partial}{\partial\varphi}\right)E_{+}^{(i)} - \frac{1}{\varrho}E_{-}^{(i)} - \left(\frac{\partial}{\partial\varrho} - \mathrm{j}\frac{1}{\varrho}\frac{\partial}{\partial\varphi}\right)E_{-}^{(i)}\right] \\
&=\; -\omega\left(\mathrm{e}^{-\mathrm{j}\varphi}\hat{\varrho}_{+}\mu_{+}^{(i)}H_{+}^{(i)} + \mathrm{e}^{\mathrm{j}\varphi}\hat{\varrho}_{-}\mu_{-}^{(i)}H_{-}^{(i)} + \mu_{z}^{(i)}H_{z}^{(i)}\hat{z}\right),
\end{aligned}
\tag{4a}
$$

and

$$
\begin{aligned}
&\hat{\varrho}_{+}\mathrm{e}^{-\mathrm{j}\varphi}\left[-\frac{\partial H_{+}^{(i)}}{\partial z} + 2^{-1/2}\left(\frac{\partial}{\partial\varrho} - \mathrm{j}\frac{1}{\varrho}\frac{\partial}{\partial\varphi}\right)H_{z}^{(i)}\right] + \hat{\varrho}_{-}\mathrm{e}^{\mathrm{j}\varphi}\left[\frac{\partial H_{-}^{(i)}}{\partial z} - 2^{-1/2}\left(\frac{\partial}{\partial\varrho} + \mathrm{j}\frac{1}{\varrho}\frac{\partial}{\partial\varphi}\right)H_{z}^{(i)}\right] \\
&+\; 2^{-1/2}\hat{z}\left[\frac{1}{\varrho}H_{+}^{(i)} + \left(\frac{\partial}{\partial\varrho} + \mathrm{j}\frac{1}{\varrho}\frac{\partial}{\partial\varphi}\right)H_{+}^{(i)} - \frac{1}{\varrho}H_{-}^{(i)} - \left(\frac{\partial}{\partial\varrho} - \mathrm{j}\frac{1}{\varrho}\frac{\partial}{\partial\varphi}\right)H_{-}^{(i)}\right] \\
&=\; \omega\left(\mathrm{e}^{-\mathrm{j}\varphi}\hat{\varrho}_{+}\varepsilon_{+}^{(i)}E_{+}^{(i)} + \mathrm{e}^{\mathrm{j}\varphi}\hat{\varrho}_{-}\varepsilon_{-}^{(i)}E_{-}^{(i)} + \varepsilon_{z}^{(i)}E_{z}^{(i)}\hat{z}\right),
\end{aligned}
\tag{4b}
$$

where $\varepsilon_{\pm}^{(i)} = \varepsilon_{0}^{(i)} \pm \varepsilon_{1}^{(i)}$, and $\mu_{\pm}^{(i)} = \mu_{0}^{(i)} \pm \mu_{1}^{(i)}$. The TCP unit vectors, $\hat{\varrho}_{\pm}$, are related to the Cartesian unit vectors $\hat{x}$ and $\hat{y}$ and to the circular cylindrical unit vectors $\hat{\varrho}$ and $\hat{\varphi}$ according to

$$\hat{\varrho}_{\pm} = 2^{-1/2}\left(\hat{\varrho} \pm \mathrm{j}\hat{\varphi}\right)\mathrm{e}^{\pm\mathrm{j}\varphi} = 2^{-1/2}\left(\hat{x} \pm \mathrm{j}\hat{y}\right). \tag{5}$$

From now, the factor $\exp\left(\mathrm{j}\omega t\right)$ will be dropped out. Maxwell divergence equations provide

$$\nabla\cdot\mathbf{E}^{(i)} = \frac{\varepsilon_{1}^{(i)}}{\varepsilon_{0}^{(i)}}\mu_{z}\omega H_{z}^{(i)} - \frac{\varepsilon_{z}^{(i)} - \varepsilon_{0}^{(i)}}{\varepsilon_{0}^{(i)}}\frac{\partial}{\partial z}E_{z}^{(i)}, \tag{6a}$$

$$\nabla\cdot\mathbf{H}^{(i)} = -\frac{\mu_{1}^{(i)}}{\mu_{0}^{(i)}}\varepsilon_{z}^{(i)}\omega E_{z}^{(i)} - \frac{\mu_{z}^{(i)} - \mu_{0}^{(i)}}{\mu_{0}^{(i)}}\frac{\partial}{\partial z}H_{z}^{(i)}. \tag{6b}$$

For the solutions proportional to $\mathrm{e}^{-\mathrm{j}\beta z}$, where β denotes the axial (or longitudinal) propagation constant, now for $E_{\pm}^{(i)} = E_{\pm}^{(i)}\left(\varrho,\varphi\right)$ and $H_{\pm}^{(i)} = H_{\pm}^{(i)}\left(\varrho,\varphi\right)$, $E_{z}^{(i)} = E_{z}^{(i)}\left(\varrho,\varphi\right)$ and $H_{z}^{(i)} = H_{z}^{(i)}\left(\varrho,\varphi\right)$, i.e.,

$$\mathbf{E}^{(i)}\left(\varrho,\varphi,z\right) = \left[\mathrm{e}^{-\mathrm{j}\varphi}\hat{\varrho}_{+}E_{+}^{(i)} + \mathrm{e}^{\mathrm{j}\varphi}\hat{\varrho}_{-}E_{-}^{(i)} + E_{z}^{(i)}\hat{z}\right]\mathrm{e}^{-\mathrm{j}\beta z}, \tag{7a}$$

$$\mathbf{H}^{(i)}\left(\varrho,\varphi,z\right) = \left[\mathrm{e}^{-\mathrm{j}\varphi}\hat{\varrho}_{+}H_{+}^{(i)} + \mathrm{e}^{\mathrm{j}\varphi}\hat{\varrho}_{-}H_{-}^{(i)} + H_{z}^{(i)}\hat{z}\right]\mathrm{e}^{-\mathrm{j}\beta z}, \tag{7b}$$

the transverse field components, $E_{\pm}^{(i)}$ and $H_{\pm}^{(i)}$, can be expressed in terms of the axial (z) components, $E_{z}^{(i)}$ and $H_{z}^{(i)}$,

$$E_{\pm}^{(i)} = \frac{-\mathrm{j}2^{-1/2}}{\omega^{2}\varepsilon_{\pm}^{(i)}\mu_{\pm}^{(i)} - \beta^{2}}\left(\frac{\partial}{\partial\varrho} \mp \mathrm{j}\frac{1}{\varrho}\frac{\partial}{\partial\varphi}\right)\left(\beta E_{z}^{(i)} \pm \mathrm{j}\omega\mu_{z}^{(i)}H_{z}^{(i)}\right), \tag{8a}$$

$$H_{\pm}^{(i)} = \frac{-\mathrm{j}2^{-1/2}}{\omega^{2}\varepsilon_{\pm}^{(i)}\mu_{\pm}^{(i)} - \beta^{2}}\left(\frac{\partial}{\partial\varrho} \mp \mathrm{j}\frac{1}{\varrho}\frac{\partial}{\partial\varphi}\right)\left(\beta H_{z}^{(i)} \mp \mathrm{j}\omega\varepsilon_{z}^{(i)}E_{z}^{(i)}\right). \tag{8b}$$

3. Helmholtz Equations

The Helmholtz wave equations in anisotropic media follow from Equation (1) and take the form [31]

$$\nabla \times \left[\tilde{\mu}^{(i)-1} \left(\nabla \times \mathbf{E}^{(i)} \right) \right] = \omega^2 \tilde{\varepsilon}^{(i)} \mathbf{E}^{(i)}, \tag{9a}$$

$$\nabla \times \left[\tilde{\varepsilon}^{(i)-1} \left(\nabla \times \mathbf{H}^{(i)} \right) \right] = \omega^2 \tilde{\mu}^{(i)} \mathbf{H}^{(i)}. \tag{9b}$$

With restrictions to the terms of zero and first order in $\mu_1^{(i)} \ll \mu_0^{(i)}$ and $\varepsilon_1^{(i)} \ll \varepsilon_0$ (including $\mu_z^{(i)} \approx \mu_0^{(i)}$ and $\varepsilon_z^{(i)} \approx \varepsilon_0$), the substitutions from Equation (4) provide

$$\left(\nabla^2 + \omega^2 \mu_0 \varepsilon_0 \right) \left(e^{-j\varphi} \hat{\varrho}_+ E_+ + e^{j\varphi} \hat{\varrho}_- E_- + E_z \hat{z} \right)$$
$$- \omega \left(\mu_0^{(i)} \varepsilon_0^{(i)} \right)^{1/2} \left(\frac{\varepsilon_1^{(i)}}{\varepsilon_0^{(i)}} + \frac{\mu_1^{(i)}}{\mu_0^{(i)}} \right) \left(\frac{\mu_0^{(i)}}{\varepsilon_0^{(i)}} \right)^{1/2} \frac{\partial}{\partial z} \left(\hat{\varrho}_+ e^{-j\varphi} H_+ + \hat{\varrho}_- e^{j\varphi} H_- + \hat{z} H_z \right) = 0, \tag{10a}$$

and

$$\left(\nabla^2 + \omega^2 \mu_0 \varepsilon_0 \right) \left(e^{-j\varphi} \hat{\varrho}_+ H_+ + e^{j\varphi} \hat{\varrho}_- H_- + H_z \hat{z} \right)$$
$$+ \omega \left(\mu_0^{(i)} \varepsilon_0^{(i)} \right)^{1/2} \left(\frac{\varepsilon_1^{(i)}}{\varepsilon_0^{(i)}} + \frac{\mu_1^{(i)}}{\mu_0^{(i)}} \right) \left(\frac{\varepsilon_0^{(i)}}{\mu_0^{(i)}} \right)^{1/2} \frac{\partial}{\partial z} \left(\hat{\varrho}_+ e^{-j\varphi} E_+ + \hat{\varrho}_- e^{j\varphi} E_- + \hat{z} E_z \right) = 0. \tag{10b}$$

Here ∇^2 denotes the Laplacian

$$\nabla^2 = \frac{\partial^2}{\partial \varrho^2} + \frac{1}{\varrho} \frac{\partial}{\partial \varrho} + \frac{1}{\varrho^2} \frac{\partial^2}{\partial \varphi^2} + \frac{\partial^2}{\partial z^2}.$$

The Helmholtz partial differential Equation (10) can be separated assuming the solutions

$$\mathbf{E}_\nu^{(i)} (\varrho, \varphi, z) = \left[e^{-j\varphi} \hat{\varrho}_+ E_{\nu+}^{(i)} (\varrho) + e^{j\varphi} \hat{\varrho}_- E_{\nu-}^{(i)} (\varrho) + E_{\nu,z}^{(i)} (\varrho) \hat{z} \right] e^{j(\nu\varphi - \beta z)}, \tag{11a}$$

$$\mathbf{H}_\nu^{(i)} (\varrho, \varphi, z) = \left[e^{-j\varphi} \hat{\varrho}_+ H_{\nu+}^{(i)} (\varrho) + e^{j\varphi} \hat{\varrho}_- H_{\nu-}^{(i)} (\varrho) + H_{\nu,z}^{(i)} (\varrho) \hat{z} \right] e^{j(\nu\varphi - \beta z)}, \tag{11b}$$

where ν is an integer. Then $\frac{\partial}{\partial z} \to -j\beta$, $\frac{\partial}{\partial \varphi} \to j\nu$. The Helmholtz equation for the electric field becomes

$$\hat{\varrho}_+ e^{-j\varphi} \left\{ \left[\left(\frac{d^2}{d\varrho^2} + \frac{1}{\varrho} \frac{d}{d\varrho} \right) + \left(\omega^2 \varepsilon_0^{(i)} \mu_0^{(i)} - \beta^2 \right) - \frac{(\nu - 1)^2}{\varrho^2} \right] E_{\nu+}^{(i)} + j\beta\omega \frac{\varepsilon_1^{(i)} \mu_0^{(i)} + \mu_1^{(i)} \varepsilon_0^{(i)}}{\varepsilon_0^{(i)}} H_{\nu+}^{(i)} \right\}$$
$$+ \hat{\varrho}_- e^{j\varphi} \left\{ \left[\left(\frac{d^2}{d\varrho^2} + \frac{1}{\varrho} \frac{d}{d\varrho} \right) + \left(\omega^2 \varepsilon_0^{(i)} \mu_0^{(i)} - \beta^2 \right) - \frac{(\nu + 1)^2}{\varrho^2} \right] E_{\nu-}^{(i)} + j\beta\omega \frac{\varepsilon_1^{(i)} \mu_0^{(i)} + \mu_1^{(i)} \varepsilon_0^{(i)}}{\varepsilon_0^{(i)}} H_{\nu-}^{(i)} \right\} \tag{12a}$$
$$+ \hat{z} \left\{ \left[\left(\frac{d^2}{d\varrho^2} + \frac{1}{\varrho} \frac{d}{d\varrho} \right) + \left(\omega^2 \varepsilon_0^{(i)} \mu_0^{(i)} - \beta^2 \right) - \frac{\nu^2}{\varrho^2} \right] E_{\nu,z}^{(i)} + j\beta\omega \frac{\varepsilon_1^{(i)} \mu_0^{(i)} + \mu_1^{(i)} \varepsilon_0^{(i)}}{\varepsilon_0^{(i)}} H_{\nu,z}^{(i)} \right\} = 0.$$

The corresponding Helmholtz equation for magnetic field is related to Equation (12a) by the duality transformation, i.e., $\mathbf{E} \to \pm\mathbf{H}$, $\mathbf{H} \to \mp\mathbf{E}$, and $\tilde{\varepsilon} \leftrightarrow \tilde{\mu}$. Then

$$
\hat{\varrho}_+ e^{-j\varphi} \left\{ \left[\left(\frac{d^2}{d\varrho^2} + \frac{1}{\varrho}\frac{d}{d\varrho} \right) + \left(\omega^2 \mu_0^{(i)} \varepsilon_0^{(i)} - \beta^2 \right) - \frac{(\nu-1)^2}{\varrho^2} \right] H_{\nu+}^{(i)} - j\beta\omega \frac{\varepsilon_1^{(i)}\mu_0^{(i)} + \mu_1^{(i)}\varepsilon_0^{(i)}}{\mu_0^{(i)}} E_{\nu+}^{(i)} \right\}
$$

$$
+ \quad \hat{\varrho}_- e^{j\varphi} \left\{ \left[\left(\frac{d^2}{d\varrho^2} + \frac{1}{\varrho}\frac{d}{d\varrho} \right) + \left(\omega^2 \mu_0^{(i)} \varepsilon_0^{(i)} - \beta^2 \right) - \frac{(\nu-1)^2}{\varrho^2} \right] H_{\nu-}^{(i)} - j\beta\omega \frac{\varepsilon_1^{(i)}\mu_0^{(i)} + \mu_1^{(i)}\varepsilon_0^{(i)}}{\mu_0^{(i)}} E_{\nu-}^{(i)} \right\} \quad (12b)
$$

$$
+ \quad \hat{z} \left\{ \left[\left(\frac{d^2}{d\varrho^2} + \frac{1}{\varrho}\frac{d}{d\varrho} \right) + \left(\omega^2 \mu_0^{(i)} \varepsilon_0^{(i)} - \beta^2 \right) - \frac{\nu^2}{\varrho^2} \right] H_{\nu,z}^{(i)} - j\beta\omega \frac{\varepsilon_1^{(i)}\mu_0^{(i)} + \mu_1^{(i)}\varepsilon_0^{(i)}}{\mu_0^{(i)}} E_{\nu,z}^{(i)} \right\} = 0.
$$

For $\varepsilon_1^{(i)} = 0$ and $\mu_1^{(i)} = 0$, Equations (12a) and (12b) represents sets of ordinary Bessel equations solved by cylindrical functions all with the same argument [30]. Equation (12a) [(12b)] contains small terms linear in $\varepsilon_1^{(i)}$ and $\mu_1^{(i)}$ proportional to the components of magnetic [electric] field. To eliminate magnetic [electric] field from Equation (12a) [(12b)], the use is made of the following procedure. In the approximation restricted to terms linear in $\mu_1^{(i)}$ and $\varepsilon_1^{(i)}$, the fields proportional to $\left(\varepsilon_1^{(i)}\mu_0^{(i)} + \mu_1^{(i)}\varepsilon_0^{(i)} \right)$ may be replaced by those in isotropic media where the solutions are given by cylindrical functions $\mathcal{Z}_\nu^{(i)} \left(\kappa_0^{(i)} \varrho \right)$ and $\mathcal{Z}_{\nu\mp1}^{(i)} \left(\kappa_0^{(i)} \varrho \right)$, i.e.,

$$
E_{\nu\pm}^{(i)} = A_{\nu\pm}^{(i)} \mathcal{Z}_{\nu\mp1}^{(i)} \left(\kappa_0^{(i)} \varrho \right), \quad E_{\nu,z}^{(i)} = A_{\nu,z}^{(i)} \mathcal{Z}_\nu^{(i)} \left(\kappa_0^{(i)} \varrho \right), \tag{13a}
$$

$$
H_{\nu\pm}^{(i)} = B_{\nu\pm}^{(i)} \mathcal{Z}_{\nu\mp1}^{(i)} \left(\kappa_0^{(i)} \varrho \right), \quad H_{\nu,z}^{(i)} = B_{\nu,z}^{(i)} \mathcal{Z}_\nu^{(i)} \left(\kappa_0^{(i)} \varrho \right). \tag{13b}
$$

Here $A_{\nu\pm}^{(i)}$ and $A_{\nu,z}^{(i)}$ denote the amplitudes of the cylindrical functions characterizing CP and z components of the electric field and $B_{\nu\pm}^{(i)}$ and $B_{\nu,z}^{(i)}$ denote the amplitudes of the cylindrical functions characterizing CP and z components of the magnetic field. The isotropic transverse propagation constant is given by $\kappa_0^{(i)} = \omega \left(\mu_0^{(i)}\varepsilon_0^{(i)} - \beta_0^2 \right)^{1/2}$. The fields are proportional to the factor $\exp\left(-j\beta_0 z \right)$, where β_0 represents the longitudinal propagation constant in an isotropic medium. Relations among the amplitudes in isotropic media summarized in Appendix A follow from the Maxwell equations in TCP cylindrical coordinate system [30].

Consequently, the magnetic field (electric field) components $\propto \left(\varepsilon_1^{(i)}\mu_0^{(i)} + \mu_1^{(i)}\varepsilon_0^{(i)} \right)$ in Equuation (12), i.e., in the equations for the electric field (magnetic field) can be taken as proportional to electric field (magnetic field) components

$$
H_z^{(i)} = -jp_z^{(i)} E_z^{(i)}, \qquad H_\pm^{(i)} = -jp_\pm^{(i)} E_\pm^{(i)}, \tag{14a}
$$

$$
E_z^{(i)} = jq_z^{(i)} H_z^{(i)}, \qquad E_\pm^{(i)} = jq_\pm^{(i)} H_\pm^{(i)}. \tag{14b}
$$

The use of Equation (14) transforms Equation (12) to sets of coupled ordinary Bessel equations.

With the abbreviations, using $\kappa^{(i)2} = \omega^2 \mu_0^{(i)} \varepsilon_0^{(i)} - \beta^2$,

$$\eta_z^{(i)2} = \kappa^{(i)2} + \beta_0 \omega \frac{\varepsilon_1^{(i)} \mu_0^{(i)} + \mu_1^{(i)} \varepsilon_0^{(i)}}{\varepsilon_0^{(i)}} p_z^{(i)}, \tag{15a}$$

$$\eta_\pm^{(i)2} = \kappa^{(i)2} + \beta_0 \omega \frac{\varepsilon_1^{(i)} \mu_0^{(i)} + \mu_1^{(i)} \varepsilon_0^{(i)}}{\varepsilon_0^{(i)}} p_\pm^{(i)}, \tag{15b}$$

$$\chi_z^{(i)2} = \kappa^{(i)2} + \beta_0 \omega \frac{\varepsilon_1^{(i)} \mu_0^{(i)} + \mu_1 \varepsilon_0^{(i)}}{\mu_0^{(i)}} q_z^{(i)}, \tag{15c}$$

$$\chi_\pm^{(i)2} = \kappa^{(i)2} + \beta_0 \omega \frac{\varepsilon_1^{(i)} \mu_0^{(i)} + \mu_1^{(i)} \varepsilon_0^{(i)}}{\mu_0^{(i)}} q_\pm^{(i)}, \tag{15d}$$

Equation (12) can be expressed in a more concise form,

$$
\begin{aligned}
& \hat{\varrho}_+ e^{-j\varphi} \left\{ \left(\frac{d^2}{d\varrho^2} + \frac{1}{\varrho} \frac{d}{d\varrho} \right) E_+^{(i)} + \left[\eta_+^{(i)2} - \frac{(\nu-1)^2}{\varrho^2} \right] E_+^{(i)} \right\} \\
+ \ & +\hat{\varrho}_- e^{j\varphi} \left\{ \left(\frac{d^2}{d\varrho^2} + \frac{1}{\varrho} \frac{d}{d\varrho} \right) E_-^{(i)} + \left[\eta_-^{(i)2} - \frac{(\nu+1)^2}{\varrho^2} \right] E_-^{(i)} \right\} \\
+ \ & \hat{z} \left[\left(\frac{d^2}{d\varrho^2} + \frac{1}{\varrho} \frac{d}{d\varrho} \right) E_z^{(i)} + \left(\eta_z^{(i)2} - \frac{\nu^2}{\varrho^2} \right) E_z^{(i)} \right] = 0,
\end{aligned}
\tag{16a}
$$

and

$$
\begin{aligned}
& \hat{\varrho}_+ e^{-j\varphi} \left\{ \left(\frac{d^2}{d\varrho^2} + \frac{1}{\varrho} \frac{d}{d\varrho} \right) H_+^{(i)} + \left[\chi_+^{(i)2} - \frac{(\nu-1)^2}{\varrho^2} \right] H_+^{(i)} \right\} \\
+ \ & +\hat{\varrho}_- e^{j\varphi} \left\{ \left(\frac{d^2}{d\varrho^2} + \frac{1}{\varrho} \frac{d}{d\varrho} \right) H_-^{(i)} + \left[\chi_-^{(i)2} - \frac{1}{\varrho^2}(\nu+1)^2 \right] H_-^{(i)} \right\} \\
+ \ & \hat{z} \left[\left(\frac{d^2}{d\varrho^2} + \frac{1}{\varrho} \frac{d}{d\varrho} \right) H_z^{(i)} + \left(\chi_z^{(i)2} - \frac{\nu^2}{\varrho^2} \right) H_z^{(i)} \right] = 0.
\end{aligned}
\tag{16b}
$$

Their solutions consist of cylindrical functions, $\mathcal{Z}_\nu^{(i)}$, with the arguments different from those in isotropic media. The solutions can be written as

$$\mathbf{E}_\nu^{(i)}(\varrho, \varphi, z) = e^{-j\varphi} \hat{\varrho}_+ A_{\nu+}^{(i)} \mathcal{Z}_{\nu-1}^{(i)} \left(\eta_+^{(i)} \varrho \right) + e^{j\varphi} \hat{\varrho}_- A_{\nu-}^{(i)} \mathcal{Z}_{\nu+1}^{(i)} \left(\eta_-^{(i)} \varrho \right) + A_{\nu,z}^{(i)} \mathcal{Z}_\nu^{(i)} \left(\eta_z^{(i)} \varrho \right) \hat{z}, \tag{17a}$$

$$\mathbf{H}_\nu^{(i)}(\varrho, \varphi, z) = e^{-j\varphi} \hat{\varrho}_+ B_{\nu+}^{(i)} \mathcal{Z}_{\nu-1}^{(i)} \left(\chi_+^{(i)} \varrho \right) + e^{j\varphi} \hat{\varrho}_- B_{\nu-}^{(i)} \mathcal{Z}_{\nu+1}^{(i)} \left(\chi_-^{(i)} \varrho \right) + B_{\nu,z}^{(i)} \mathcal{Z}_\nu^{(i)} \left(\chi_z^{(i)} \varrho \right) \hat{z}, \tag{17b}$$

Here, the factor $\exp[j(\nu\varphi - \beta z)]$ was dropped out. The relations among the amplitudes are given by Equation (4). In particular, according to Equation (8), the TCP components $E_{\nu\pm}^{(i)}$ and $H_{\nu\pm}^{(i)}$ in Equation (11) can conveniently be expressed in terms of $A_{\nu,z}^{(i)}$ and $B_{\nu,z}^{(i)}$,

$$E_{\nu\pm}^{(i)} = \frac{2^{-1/2}}{\kappa_\pm^{(i)2}} \left[\omega \mu_\pm^{(i)} B_{\nu,z}^{(i)} \chi_z^{(i)} \mathcal{Z}_{\nu\mp1}^{(i)} \left(\chi_z^{(i)} \varrho \right) \mp j\beta A_{\nu,z}^{(i)} \eta_z^{(i)} \mathcal{Z}_{\nu\mp1}^{(i)} \left(\eta_z^{(i)} \varrho \right) \right], \tag{18a}$$

$$H_{\nu\pm}^{(i)} = \frac{2^{-1/2}}{\kappa_\pm^{(i)2}} \left[-\omega \varepsilon_\pm^{(i)} A_{\nu,z}^{(i)} \eta_z^{(i)} \mathcal{Z}_{\nu\mp1}^{(i)} \left(\eta_z^{(i)} \varrho \right) \mp j\beta B_{\nu,z}^{(i)} \chi_z^{(i)} \mathcal{Z}_{\nu\mp1}^{(i)} \left(\chi_z^{(i)} \varrho \right) \right], \tag{18b}$$

where $\kappa_\pm^{(i)2} = \omega^2 \mu_\pm^{(i)} \varepsilon_\pm^{(i)} - \beta^2$.

4. A Simple Cylindrically Layered Structure

The structure consists of a core in the region $0 \leq \varrho \leq a$ characterized by $\tilde{\varepsilon}^{(1)}$ and $\tilde{\mu}^{(1)}$, and a cladding in the region $a \leq \varrho$ characterized by $\tilde{\varepsilon}^{(2)}$ and $\tilde{\mu}^{(2)}$ (Figure 1). To operate as a waveguide, the general solutions, Equation (17), of Equation (16) are replaced in the core by a set of Bessel functions of first kind, i.e., $\mathcal{Z}_\nu^{(1)}\left(\chi_z^{(1)}\varrho\right) = \mathcal{J}_\nu\left(\chi_z^{(1)}\varrho\right)$ and $\mathcal{Z}_\nu^{(1)}\left(\eta_z^{(1)}\varrho\right) = \mathcal{J}_\nu\left(\eta_z^{(1)}\varrho\right)$. In the cladding, the acceptable solutions are given by a set of modified Bessel functions of third kind deduced from $\mathcal{Z}_\nu^{(2)}\left(\chi_z^{(2)}\varrho\right) = j^{-\nu-1}\frac{2}{\pi}\mathcal{K}_\nu(\xi_z^{(2)}\varrho)$ and $\mathcal{Z}_\nu^{(2)}\left(\eta_z^{(2)}\varrho\right) = j^{-\nu-1}\frac{2}{\pi}\mathcal{K}_\nu\left(\zeta_z^{(2)}\varrho\right)$ for $\eta_z^{(2)} = j\zeta_z^{(2)}$ and $\chi_z^{(2)} = j\xi_z^{(2)}$. It is convenient to introduce the effective index of refraction, $N = \beta\lambda_{\text{vac}}/(2\pi)$, the relative magnetic permeability, $\kappa_{m\pm}^{(i)} = \mu_\pm^{(i)}/\mu_{\text{vac}}$, and the relative electric permittivity, $\kappa_{e\pm}^{(i)} = \varepsilon_\pm^{(i)}/\varepsilon_{\text{vac}}$. The squared transverse propagation, $\kappa_\pm^2$, and attenuation, $\gamma_\pm^2$, constants are defined as,

$$\kappa_\pm^{(1)2} = \left(\frac{2\pi}{\lambda_{\text{vac}}}\right)^2\left(\kappa_{m\pm}^{(1)}\kappa_{e\pm}^{(1)} - N^2\right) \equiv \kappa_\pm^2, \tag{19a}$$

$$\kappa_\pm^{(2)2} = \left(\frac{2\pi}{\lambda_{\text{vac}}}\right)^2\left(\kappa_{m\pm}^{(2)}\kappa_{e\pm}^{(2)} - N^2\right) \equiv -\gamma_\pm^2. \tag{19b}$$
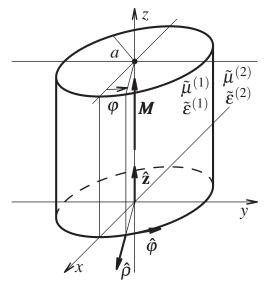

Figure 1. Dielectric circular cylindrical waveguide with the axial magnetization, **M**, in a circular cylinder coordinate system with the unit vectors $\hat{\varrho}$, $\hat{\varphi}$, and $\hat{z}$. A field point is specified by $\varrho = \sqrt{x^2 + y^2}$, φ, and z. The core region of the radius a, $\varrho \leq a$, is characterized by the permeability and permittivity tensors, $\tilde{\mu}^{(1)}$ and $\tilde{\varepsilon}^{(1)}$. The cladding region, $\varrho \geq a$, is characterized by the permeability and permittivity tensors, $\tilde{\mu}^{(2)}$ and $\tilde{\varepsilon}^{(2)}$.

The symbols λ_{vac}, μ_{vac}, and ε_{vac} denote the radiation wavelength, magnetic permeability, and electric permittivity in a vacuum, respectively. Deduced from the boundary conditions at the interface $\varrho = a$, the eigenvalue equation takes the form,

$$
\begin{aligned}
N^2 & \left\{ \mathcal{K}_\nu \left(\zeta_z^{(2)} a \right) \left[\frac{1}{\kappa_+^2} \mathcal{J}_{\nu-1} \left(\eta_z^{(1)} a \right) + \frac{1}{\kappa_-^2} \mathcal{J}_{\nu+1} \left(\eta_z^{(1)} a \right) \right] \eta_z^{(1)} \right. \\
& \left. - \mathcal{J}_\nu \left(\eta_z^{(1)} a \right) \left[\frac{1}{\gamma_+^2} \mathcal{K}_{\nu-1} (\zeta_z^{(2)} a) - \frac{1}{\gamma_-^2} \mathcal{K}_{\nu+1} (\zeta_z^{(2)} a) \right] \zeta_z^{(2)} \right\} \\
& \times \left\{ \mathcal{K}_\nu (\xi_z^{(2)} a) \left[\frac{1}{\kappa_+^2} \mathcal{J}_{\nu-1} \left(\chi_z^{(1)} a \right) + \frac{1}{\kappa_-^2} \mathcal{J}_{\nu+1} \left(\chi_z^{(1)} a \right) \right] \chi_z^{(1)} \right. \\
& \left. - \mathcal{J}_\nu \left(\chi_z^{(1)} a \right) \left[\frac{1}{\gamma_+^2} \left[\mathcal{K}_{\nu-1} (\xi_z^{(2)} a) \right] - \frac{1}{\gamma_-^2} \mathcal{K}_{\nu+1} (\xi_z^{(2)} a) \right] \xi_z^{(2)} \right\} \\
& - \left\{ \mathcal{K}_\nu \left(\zeta_z^{(2)} a \right) \left[\frac{\kappa_{e+}^{(1)}}{\kappa_+^2} \mathcal{J}_{\nu-1} \left(\eta_z^{(1)} a \right) - \frac{\kappa_{e-}^{(1)}}{\kappa_-^2} \mathcal{J}_{\nu+1} \left(\eta_z^{(1)} a \right) \right] \eta_z^{(1)} \right. \\
& \left. - \mathcal{J}_\nu \left(\eta_z^{(1)} a \right) \left[\frac{\kappa_{e+}^{(2)}}{\gamma_+^2} \mathcal{K}_{\nu-1} (\zeta_z^{(2)} a) + \frac{\kappa_{e-}^{(2)}}{\gamma_-^2} \mathcal{K}_{\nu+1} (\zeta_z^{(2)} a) \right] \zeta_z^{(2)} \right\} \\
& \times \left\{ \mathcal{K}_\nu (\xi_z^{(2)} a) \left[\frac{\kappa_{m+}^{(1)}}{\kappa_+^2} \mathcal{J}_{\nu-1} \left(\chi_z^{(1)} a \right) - \frac{\kappa_{m-}^{(1)}}{\kappa_-^2} \mathcal{J}_{\nu+1} \left(\chi_z^{(1)} a \right) \right] \chi_z^{(1)} \right. \\
& \left. - \mathcal{J}_\nu \left(\chi_z^{(1)} a \right) \left[\frac{\kappa_{m+}^{(2)}}{\gamma_+^2} \mathcal{K}_{\nu-1} (\xi_z^{(2)} a) + \frac{\kappa_{m-}^{(2)}}{\gamma_-^2} \mathcal{K}_{\nu+1} (\xi_z^{(2)} a) \right] \xi_z^{(2)} \right\} \\
& = 0.
\end{aligned}
\tag{20}
$$

It remains to specify the arguments of the cylindrical functions. These require the eigenvalue of the effective index of refraction, i.e., effective guide index, $N_0 = \beta_0 \lambda_{\text{vac}} / (2\pi)$, obtained from Equation (20) for the special case of isotropic core and cladding. Using the recursion relations [32] given in Appendix B, one indeed arrives at the eigenvalue equation in isotropic circular cylindrical waveguides [11,33] extended by Kong to the case of both $\varepsilon_0^{(i)} \neq \varepsilon_{\text{vac}}$ and $\mu_0^{(i)} \neq \mu_{\text{vac}}$, [34] here expressed as

$$
\left(\nu N_0 \frac{\kappa_0^2 a^2 + \gamma_0^2 a^2}{\kappa_0^2 a^2 \gamma_0^2 a^2} \right)^2 = \mathcal{G}_{m0} \mathcal{G}_{e0},
\tag{21}
$$

where $\kappa_0^{(1)2} = \kappa_0^2$, $\kappa_0^{(2)2} = -\gamma_0^2$, and

$$
\mathcal{G}_{m0} = \frac{\kappa_{m0}^{(1)}}{\kappa_0 a} \frac{\mathcal{J}_{\nu-1}(\kappa_0 a) - \mathcal{J}_{\nu+1}(\kappa_0 a)}{2 \mathcal{J}_\nu(\kappa_0 a)} - \frac{\kappa_{m0}^{(2)}}{\gamma_0 a} \frac{\mathcal{K}_{\nu-1}(\gamma_0 a) + \mathcal{K}_{\nu+1}(\gamma_0 a)}{2 \mathcal{K}_\nu(\gamma_0 a)},
\tag{22a}
$$

$$
\mathcal{G}_{e0} = \frac{\kappa_{e0}^{(1)}}{\kappa_0 a} \frac{\mathcal{J}_{\nu-1}(\kappa_0 a) - \mathcal{J}_{\nu+1}(\kappa_0 a)}{2 \mathcal{J}_\nu(\kappa_0 a)} - \frac{\kappa_{e0}^{(2)}}{\gamma_0 a} \frac{\mathcal{K}_{\nu-1}(\gamma_0 a) + \mathcal{K}_{\nu+1}(\gamma_0 a)}{2 \mathcal{K}_\nu(\gamma_0 a)}.
\tag{22b}
$$

The continuity of the z-field components requires $p_z^{(1)} = p_z^{(2)} = p_z$ and $q_z^{(1)} = q_z^{(2)} = q_z$ with

$$
p_z = \frac{-\kappa_0^2 a^2 \gamma_0^2 a^2}{\nu N_0 (\kappa_0^2 a^2 + \gamma_0^2 a^2)} \left(\frac{\varepsilon_{\text{vac}}}{\mu_{\text{vac}}} \right)^{1/2} \mathcal{G}_{e0},
\tag{23a}
$$

$$
q_z = \frac{-\kappa_0^2 a^2 \gamma_0^2 a^2}{\nu N_0 (\kappa_0^2 a^2 + \gamma_0^2 a^2)} \left(\frac{\mu_{\text{vac}}}{\varepsilon_{\text{vac}}} \right)^{1/2} \mathcal{G}_{m0}.
\tag{23b}
$$

Please note that their product obeys $p_z q_z = 1$, which is another way to represent the eigenvalue equation, Equation (21). In Equation (20), the arguments of the Bessel functions for the core become

$$\eta_z^{(1)} = \left(\frac{2\pi}{\lambda_{\text{vac}}}\right)\left[\kappa_{e0}^{(1)}\kappa_{m0}^{(1)} - N^2 - \frac{\kappa_{e1}^{(1)}\kappa_{m0}^{(1)} + \kappa_{m1}^{(1)}\kappa_{e0}^{(1)}}{\kappa_{e0}^{(1)}}\frac{\nu N_0\left(\kappa_0^2 a^2 + \gamma_0^2 a^2\right)}{\kappa_0^2 a^2 \gamma_0^2 a^2}\mathcal{G}_{m0}^{-1}\right]^{1/2} \tag{24a}$$

$$\chi_z^{(1)} = \left(\frac{2\pi}{\lambda_{\text{vac}}}\right)\left[\kappa_{e0}^{(1)}\kappa_{m0}^{(1)} - N^2 - \frac{\kappa_{e1}^{(1)}\kappa_{m0}^{(1)} + \kappa_{m1}^{(1)}\kappa_{e0}^{(1)}}{\kappa_{m0}^{(1)}}\frac{\nu N_0\left(\kappa_0^2 a^2 + \gamma_0^2 a^2\right)}{\kappa_0^2 a^2 \gamma_0^2 a^2}\mathcal{G}_{e0}^{-1}\right]^{1/2} \tag{24b}$$

and the arguments of modified Bessel functions for the cladding become

$$\zeta_z^{(2)} = \left(\frac{2\pi}{\lambda_{\text{vac}}}\right)\left[N^2 - \kappa_{e0}^{(2)}\kappa_{m0}^{(2)} + \frac{\kappa_{e1}^{(2)}\kappa_{m0}^{(2)} + \kappa_{m1}^{(2)}\kappa_{e0}^{(2)}}{\kappa_{e0}^{(2)}}\frac{\nu N_0\left(\kappa_0^2 a^2 + \gamma_0^2 a^2\right)}{\kappa_0^2 a^2 \gamma_0^2 a^2}\mathcal{G}_{m0}^{-1}\right]^{1/2} \tag{24c}$$

$$\xi_z^{(2)} = \left(\frac{2\pi}{\lambda_{\text{vac}}}\right)\left[N^2 - \kappa_{e0}^{(2)}\kappa_{m0}^{(2)} + \frac{\kappa_{e1}^{(2)}\kappa_{m0}^{(2)} + \kappa_{m1}^{(2)}\kappa_{e0}^{(2)}}{\kappa_{m0}^{(2)}}\frac{\nu N_0\left(\kappa_0^2 a^2 + \gamma_0^2 a^2\right)}{\kappa_0^2 a^2 \gamma_0^2 a^2}\mathcal{G}_{e0}^{-1}\right]^{1/2} \tag{24d}$$

Here $\kappa_{e\pm}^{(i)} = \kappa_{e0}^{(i)} \pm \kappa_{e1}^{(i)}$, $\kappa_{m\pm}^{(i)} = \kappa_{m0}^{(i)} \pm \kappa_{m1}^{(i)}$, $i = 1, 2$, denote the CP relative permittivities and relative permeabilities in the core ($i = 1$) and in the cladding ($i = 2$). The evaluation of Equation (20) confirms that there are no first order effects of $\varepsilon_1^{(1)}$, $\mu_1^{(1)}$, $\varepsilon_1^{(2)}$, or $\mu_1^{(2)}$ on N for $\nu = 0$, i.e., for TE and TM modes, as expected [14,35].

Solutions to the eigenvalue equation, Equation (20), will now be illustrated on a circular cylindrical dielectric waveguide operating at the wavelength $\lambda_{\text{vac}} = 1.550$ μm with the core made from yttrium iron garnet, $Y_3Fe_5O_{12}$ (YIG), and the cladding made from gallium substituted YIG, $Y_3Fe_{5-x}Ga_xO_{12}$ (GaYIG). The material parameters as functions of the diamagnetic substitution are collected in Table 1. Their choice was inspired by the situations in pure and gallium substituted yttrium iron garnets [36,37].

Table 2 provides the summary of parameters in the isotropic waveguide ($\kappa_{e1}^{(i)} = \kappa_{m1}^{(i)} = 0$). The waveguide consists of a core of refractive index $n_1 = 2.200$ and a cladding of refractive index $n_2(x) < n_1$ monotonously decreasing with the diamagnetic substitution, x. The choice of $V-$number, i.e., $V = (2\pi/\lambda_{\text{vac}})\,\Delta a = (2\pi/\lambda_{\text{vac}})\left(n_1^2 - n_2^2\right)^{1/2} a \approx 2.400 < 2.405$ for all x corresponds to monomode regime. This requires a corresponding adjustment of a, the core radius. Figure 2 shows the dependence of a and Δ on x.

Table 2 further contains the solution to the isotropic eigenvalue equation, Equation (21), N_0, and the penetration depth in the cladding, $\delta = \lambda_{\text{vac}} / (2\pi)\left(N_0^2 - n_2^2\right)^{-1/2}$, a parameter useful in the evaluation of waveguide cross section. Figure 3 shows the effect of x on the effective guide index, N_0, and the refractive index in the cladding, n_2.

The eigenvalues $N_\pm \propto \beta_\pm$ distinguish the solutions to Equation (20). Here N_+ denotes the solution for $\nu = +1$ ($\kappa_{e1}^{(i)} > 0$ and $\kappa_{m1}^{(i)} > 0$, $i = 1, 2$), N_- denotes that for $\nu = -1$ ($\kappa_{e1}^{(i)} > 0$ and $\kappa_{m1}^{(i)} > 0$). The magnetization reversal results in the exchange of N_+ and N_-. For example, at $\nu = +1$ for $-\kappa_{e1}^{(i)} > 0$ and $-\kappa_{m1}^{(i)} > 0$ (corresponding to the magnetization reversal, $M \to -M$), the solution is N_-. The eigenvalue N_0 in the isotropic waveguide ($\kappa_{e1}^{(i)} = 0$ and $\kappa_{m1}^{(i)} = 0$, corresponding to $M = 0$) takes the same value for $\nu = \pm 1$.

The forward ($\beta_\pm > 0$) propagation was assumed with $N_\pm > 0$. The eigenvalues $-N_\pm > 0$ of Equation (20) represent the solutions for the reversed propagation ($-\beta_\pm > 0$). The propagation reversal does not change $|N_\pm|$ the absolute values of $N_\pm$, as required for the nonreciprocal propagation.

The eigenvalue difference, $(N_+ - N_-) \propto (\beta_+ - \beta_-)$, a measure of nonreciprocity, as a function of x was computed for two cases, i.e., for a magnetic core and a nonmagnetic cladding, denoted as ΔN_{co}

and for the magnetic core and magnetic cladding, denoted as ΔN. A considerable enhancement of $(N_+ - N_-)$ is predicted in the latter case. The trends are shown in Figure 4.
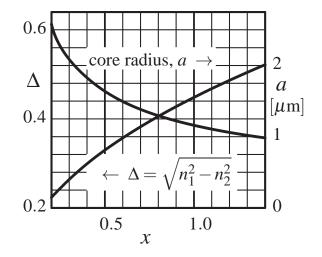

Figure 2. The core radius, a, and the parameter, $\Delta = \sqrt{n_1^2 - n_2^2}$, in a monomode dielectric cylindrical waveguide as a function of Ga content, x, in yttrium iron garnet, $Y_3Fe_{5-x}Ga_xO_{12}$, in the cladding. The symbols n_1 and n_2 denote the indices of refraction in the core and in the cladding, respectively. The $V-$number was fixed at $V = 2.400$.
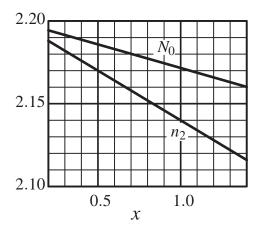

Figure 3. The effective guide index, N_0 and the refractive index, n_2, of the cladding in a monomode isotropic dielectric cylindrical waveguide as a function of Ga content, x, in $Y_3Fe_{5-x}Ga_xO_{12}$, forming the cladding.

In the waveguide with the nonmagnetic cladding, the distance $d = \lambda_{vac} / [4(N_+ - N_-)]$ required for the azimuth rotation on the axis $\varrho = 0$ by $\pi/4$ remains practically independent of x, $d \approx 198$ μm. On the other hand, in the waveguide with magnetic core and magnetic cladding, the required d is reduced to $d \approx 140$ μm for $x = 0.2$. The results are collected in Table 3.

In practice, it would be desirable to reduce Ga content and consequently Δ. This would enable the monomode regime at a higher core radius and at a higher Curie temperature in the cladding. As indicated in Figure 4, this would also increase the magnetooptic contribution from the cladding and improve the weak guiding regime with reduced axial field components. The characteristics were evaluated for the core made of YIG. The Ce^{3+} substitution for Y^{3+} in $Ce_yY_{3-y}Fe_5O_{12}$ iron garnets can significantly improve magnetooptic activity at the communication wavelength 1.55 μm with respect to that in YIG [38].
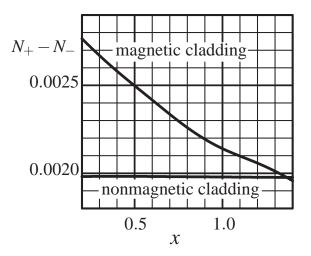
Figure 4. Difference in effective guide indices, $N_+ - N_-$, for the $\pm$ transverse circular polarizations in a monomode dielectric circular cylindrical waveguide with the axial magnetization as a function of Ga content, x, in yttrium iron garnet, $Y_3Fe_{5-x}Ga_xO_{12}$, in the cladding. $N_+ - N_-$ is plotted for two cases: (1) For the case where both the core and the cladding are characterized by the permittivity and permeability tensors (magnetic cladding). (2) For the case where the core remains characterized by the permittivity and permeability tensors while the isotropic cladding is characterized by scalar permittivity and permeability (nonmagnetic cladding).

Table 1. Effect of diamagnetic substitution, x, in yttrium iron garnet, $Y_3Fe_{5-x}Ga_xO_{12}$, on the real index of refraction, n, relative magnetization, $\overline{M}$, and the off-diagonal relative permittivity and permeability tensor elements, κ_{e1} and κ_{m1}.

x	0	0.2	0.4	0.6	0.8	1.0	1.2	1.4
n	2.200	2.188	2.176	2.164	2.152	2.140	2.128	2.116
$\overline{M}$	1	0.806	0.617	0.450	0.289	0.167	0.083	-0.022
$\kappa_{e1} \times 10^3$	2	1.611	1.233	0.90	0.578	0.333	0.167	-0.044
$\kappa_{m1} \times 10^3$	1	0.806	0.617	0.450	0.289	0.167	0.083	-0.022

Table 2. Effect of diamagnetic substitution, x, in yttrium iron garnet $Y_3Fe_{5-x}Ga_xO_{12}$ on the waveguide parameters: the cladding index of refraction, n_2, $\Delta = \sqrt{n_1^2 - n_2^2}$, the effective guide index at $M = 0$, N_0, V—number, the core radius, a, and the penetration depth in the cladding, δ.

x	0.2	0.4	0.6	0.8	1.0	1.2	1.4
n_2	2.188	2.176	2.164	2.152	2.140	2.128	2.116
Δ	0.229469	0.324074	0.396363	0.457051	0.510294	0.558226	0.602116
V	2.40082	2.40011	2.40045	2.39929	2.39953	2.39863	2.39929
a [μm]	2.581	1.827	1.494	1.295	1.160	1.060	0.983
N_0	2.19435	2.18869	2.18302	2.17732	2.17162	2.16589	2.16017
δ [μm]	1.479	1.048	0.858	0.745	0.668	0.6116	0.568

Table 3. Effect of diamagnetic substitution, x, in yttrium iron garnet $Y_3Fe_{5-x}Ga_xO_{12}$ on the difference in effective guide indices in a waveguide with nonmagnetic cladding, ΔN_{co}, on the difference in effective guide indices in the waveguide with magnetic cladding, ΔN, and on the distance, d, required for the phase shift $\pi/4$.

x	0.2	0.4	0.6	0.8	1.0	1.2	1.4
$\Delta N_{co} \times 10^3$	1.98134	1.98262	1.98182	1.98028	1.97902	1.97756	1.97642
$\Delta N \times 10^3$	2.76591	2.58059	2.41696	2.25978	2.14032	2.05772	1.95713
d [μm]	140.099	150.159	160.325	171.477	181.048	188.315	197.994

5. Conclusions

Magnetooptics in circular cylindrical structures was treated in terms of the Helmholtz vector wave equation for axially magnetized media characterized by electric permittivity and magnetic permeability tensors. In TCP components the Helmholtz vector wave equations splits into three ordinary differential equations. With the restriction to the magnetooptic effects linear in the off-diagonal tensor elements, their solutions were expressed analytically and applied to nonreciprocal guiding in dielectric circular cylindrical waveguides.

The eigen value equation deduced from the boundary conditions at the core—cladding interface provided the propagation parameters for guided modes. It displays the symmetry imposed by the electric permittivity and magnetic permeability tensors for axially magnetized cylindrical waveguides. There are no first order effects on the TE and TM modes and the weak guidance approximation is included as a limiting case.

Numerical evaluations of magnetooptic waveguides showed that fiber compatible nonreciprocal devices using yttrium iron garnets with controlled gallium concentration display reasonable magnetooptic characteristics at the propagation distance of $\sim 10^2$ μm.

The analysis may be applied to optimization of magnetooptic waveguides, fiber sensors of currents and magnetic fields, and to the evaluation of magnetic field effects in fiber gyroscopes [39–43]. The approach may be extended to nonreciprocal multilayer and graded circular cylindrical waveguides, nonreciprocal plasmonic waveguides, nonreciprocal cylindrical waveguides of (near) square cross sections [44–48], circular waveguide structures containing cylindrically anisotropic metamaterials [49], and waveguides displaying optical activity [50]. From the analytical point of view, the problem is similar to that of cylindrical quantum potential well with penetrable walls [51].

Conflicts of Interest: The author declare no conflict of interest.

Appendix A. Relations among Amplitudes

Relations among the amplitudes in isotropic cylindrical media [30] defined in Equation (13) for the fields proportional to the factor $e^{j(\nu\varphi - \beta_0 z)}$ follow from the Maxwell Equation (4) reduced to the scalar $\varepsilon_0^{(i)}$ and $\mu_0^{(i)}$

$$
\begin{pmatrix}
-\omega\varepsilon_0^{(i)} & 0 & 0 & j\beta_0 & 0 & 2^{-1/2}\kappa_0^{(i)} \\
0 & \omega\varepsilon_0^{(i)} & 0 & 0 & j\beta_0 & -2^{-1/2}\kappa_0^{(i)} \\
0 & 0 & \omega\varepsilon_0^{(i)} & 2^{-1/2}\kappa_0^{(i)} & 2^{-1/2}\kappa_0^{(i)} & 0 \\
j\beta_0 & 0 & 2^{-1/2}\kappa_0^{(i)} & \omega\mu_0^{(i)} & 0 & 0 \\
0 & -j\beta_0 & 2^{-1/2}\kappa_0^{(i)} & 0 & \omega\mu_0^{(i)} & 0 \\
2^{-1/2}\kappa_0^{(i)} & 2^{-1/2}\kappa_0^{(i)} & 0 & 0 & 0 & -\omega\mu_0^{(i)}
\end{pmatrix}
\begin{pmatrix}
A_{\nu+}^{(i)} \\
A_{\nu-}^{(i)} \\
A_{\nu,z}^{(i)} \\
B_{\nu+}^{(i)} \\
B_{\nu-}^{(i)} \\
B_{\nu,z}^{(i)}
\end{pmatrix} = 0.
$$

Appendix B. Recursion Relations

Appendix B lists the recursion relations [31] for the Bessel functions of first kind, $\mathcal{J}_\nu\left(\chi_z^{(1)}\varrho\right)$,

$$\mathcal{J}_\nu'(\kappa\varrho) = \frac{\mathrm{d}\mathcal{J}_\nu(\kappa\varrho)}{\mathrm{d}(\kappa\varrho)} = \frac{1}{2}\left[\mathcal{J}_{\nu-1}(\kappa\varrho) - \mathcal{J}_{\nu+1}(\kappa\varrho)\right],$$

$$\frac{2\nu}{\kappa\varrho}\mathcal{J}_\nu(\kappa\varrho) = \mathcal{J}_{\nu-1}(\kappa\varrho) - \mathcal{J}_{\nu+1}(\kappa\varrho),$$

and for the modified Bessel functions of third kind, $\mathcal{K}_\nu(\gamma\varrho)$,

$$\mathcal{K}_\nu'(\gamma\varrho) = \frac{\mathrm{d}\mathcal{K}_\nu(\gamma\varrho)}{\mathrm{d}(\gamma\varrho)} = -\frac{1}{2}\left[\mathcal{K}_{\nu-1}(\gamma\varrho) + \mathcal{K}_{\nu+1}(\gamma\varrho)\right],$$

$$-\frac{2\nu}{\gamma\varrho}\mathcal{K}_\nu(\gamma\varrho) = \mathcal{K}_{\nu-1}(\gamma\varrho) - \mathcal{K}_{\nu+1}(\gamma\varrho).$$

References

1. Collin, R.E. *Foundation for Microwave Engineering*, 2nd ed.; Wiley Interscience: New York, NY, USA, 2001; pp. 450–476, ISBN 0-7803-6031-1.
2. Yeh, P. Optics of anisotropic layered media: A new 4×4 matrix algebra. *Surf. Sci.* **1980**, *96*, 41–53. [CrossRef]
3. Gismyatov, I.F.; Sementsov, D.I. Magneto-Optical Effects upon Reflection of Light from a Ferrodielectric with an Arbitrary Orientation of Magnetization. *Opt. Spectrosc.* **2002**, *92*, 588–592. [CrossRef]
4. Bukhanko, A.F. Effects of Nonreciprocity in Structure with Noncollinear Orientation of Magnetization of Layers. *Opt. Spectrosc.* **2011**, *110*, 281–286. [CrossRef]
5. Tabor, W.J.; Chen F.S. Electromagnetic Propagation through Materials Possessing Both Faraday Rotation and Birefringence: Experiments with Ytterbium Orthoferrite. *J. Appl. Phys.* **1969**, *40*, 2760–2765. [CrossRef]
6. Tien, P.K. Integrated optics and new wave phenomena in optical waveguides. *Rev. Mod. Phys.* **1977**, *49*, 361–419. [CrossRef]
7. Stadler, B.J.H.; Mizumoto, T. Integrated Magneto-Optical Materials and Isolators: A Review. *IEEE Photonics J.* **2014**, *6*, 0600215. [CrossRef]
8. Gloge, D. Weakly guiding fibers. *Appl. Opt.* **1971**, *10*, 2252–2258. [CrossRef] [PubMed]
9. Marcuse, D. *Theory of Dielectric Optical Waveguides*; Academic Press: New York, NY, USA; London, UK, 1974; Chapter 2, pp. 60–78, ISBN 0-12-470950-8.
10. Snyder, A.W. Understanding Monomode Optical Fibers. *Proc. IEEE* **1981**, *69*, 6–13. [CrossRef]
11. Snyder A.W.; Love, J.D. *Optical Waveguide Theory*; Chapman & Hall: London, UK; New York, NY, USA; Tokyo, Japan; Mebourne, Australia; Madras, India, 1991; Chapter 11, pp. 220–226; Chapter 13, pp. 280–290, ISBN 0-412-24250-8.
12. Yoshino, T. Theory for the Faraday effect in optical fiber. *J. Opt. Soc. Am. B* **2005**, *22*, 1856–1860. [CrossRef]
13. Bozinovic, N.; Golowich, S.; Kristensen, P.; Ramachandran, S. Control of orbital angular momentum of light with optical fibers. *Opt. Lett.* **2012**, *37*, 2451–2453. [CrossRef]
14. Kales, M.L. Modes in Wave Guides Containing Ferrites. *J. Appl. Phys.* **1954**, *24*, 604–608. [CrossRef]
15. Fallahkhair, A.B.; Li, K.S.; Murphy, T.E. Vector Finite Difference Modesolver for Anisotropic Dielectric Waveguides. *J. Ligthtw. Technol.* **2008**, *26*, 1423–1431. [CrossRef]
16. Pintus, P. Accurate vectorial finite element mode solver for magneto-optic and anisotropic waveguides. *Opt. Express* **2014**, *22*, 15737–15756. [CrossRef]
17. Epstein, P.S. Theory of Wave Propagation in a Gyromagnetic Medium. *Rev. Mod. Phys.* **1956**, *28*, 3–17. [CrossRef]
18. Landau, L.D.; Lifschitz, E.M. *Electrodynamique de Milieux Continus*; Editions Mir: Moscou, Russia, 1969; Chapitre XI, pp. 429–438.
19. Pershan, P.S. Magneto-optical effects. *J. Appl. Phys.* **1967**, *38*, 1482–1490. [CrossRef]
20. Freiser, M.J. A Survey of Magnetooptical Effects. *IEEE Trans. Magn.* **1968**, *4*, 152–161. [CrossRef]

21. Dillon, J.F., Jr. Origin and Uses of the Faraday Rotation in Magnetic Crystals. *J. Appl. Phys.* **1968**, *39*, 922–929. [CrossRef]

22. Suits, J.C. Faraday and Kerr Effects in Magnetic Compounds. *IEEE Trans. Magn.* **1972**, *8*, 95–105. [CrossRef]

23. Wettling, W. Magneto-optics in ferrites. *J. Magn. Magn. Mater.* **1976**, *3*, 147–160. [CrossRef]

24. Wangsness, R.K. Susceptibility Tensor and the Faraday Effect in Ferrimagnets. *Phys. Rev.* **1954**, *95*, 339–345. [CrossRef]

25. Krinchik, G.S.; Chetkin, M.V. The problem of determining the dielectric perfmittivity and magnetic permeability tensors of a medium. *Sov. Phys. JETP* **1959**, *36*, 1368–1369.

26. Krinchik, G.S.; Chetkin, M.V. Exchange interaction and magneto-optical effects in ferrite garnets. *Sov. Phys. JETP* **1962**, *14*, 485–703.

27. Chetkin, M.V.; Shalygin, A.N. The Faraday Effect in Garnets in the Infrared Region. *J. Appl. Phys.* **1968**, *39*, 561–562. [CrossRef]

28. Krinchik, G.S.; Gushchin, V.S.; Tsidaeva, N.I. Temperature-independent Faraday effect in rare-earth iron garnets. *Sov. Phys. JETP* **1984**, *59*, 410–414.

29. Druzhinin, A.V.; Lobov, I.D.; Mayevskiy, V.M. A new gyromagnetic effect in the optical frequency range. *Pis. Zh. Tekh. Fiz.* **1985**, *11*, 879–882.

30. Višňovský, Š. Helmholtz Equation in Transverse Circular Representation. *Prog. Electromagn. Res. M* **2017**, *59*, 161–170. [CrossRef]

31. Chew, W.C. *Waves and Fields in Inhomogeneous Media*; Series on Electromagnetic Waves; IEEE Press: New York, NY, USA, 1995; Chapter 1, p. 22, ISBN 0-7803-4749-8.

32. Arfken, G.B.; Weber, H.J. *Mathematical Methods for Physicists*; Elsevier Academic Press: Burlington, NJ, USA; San Diego, CA, USA; London, UK, 2005; Chapters 2, 9 and 11, ISBN 0-12-088584-0.

33. Marcuse, D. *Light Transmission Optics*; Van Nostrand Reinhold Company: London, UK; Toronto, ON, Canada; Melbourne, Australia, 1972; Chapter 8, pp. 288–305.

34. Kong, J.A. *Electromagnetic Wave Theory*; EMW Publishing: Cambridge, MA, USA, 2000; Chapter 3, pp. 450–460, ISBN 0-9668143-9-8.

35. Anderson N.R.; Camley, R.E. Multilayer magnetic waveguides: Optimizing nonreciprocal propagation. *J. Appl. Phys.* **2014**, *116*, 023903. [CrossRef]

36. Cooper, R.W.; Crossley, W.A.; Page, J.L.; Pearson, R.F. Faraday Rotation in YIG and TbIG. *J. Appl. Phys.* **1968**, *39*, 565–567. [CrossRef]

37. Doormann, V.; Krumme, J.-P.; Lenz, H. Optical and magneto-optical tensor spectra of bismuth substituted yttrium iron garnet films. *J. Appl. Phys.* **1990**, *68*, 3544–3553. [CrossRef]

38. Sekijima, T.; Funakoshi, T.; Katabe, K.; Tahara, K.; Fujii, T.; Wakino, K.; Okada, M. Growth and Optical Properties of Ce-substituted Fibrous YIG Single Crystals. *Jpn. J. Appl. Phys.* **1998**, *37*, 4854–4857. [CrossRef]

39. Dulal, P.; Block, A.D.; Gage, T.E.; Haldren, H.A.; Sung, S.-Y.; Hutchings, D.C.; Stadler, B.J.H. Optimized Magneto-optical Isolator Designs Inspired by Seedlayer-Free Terbium Iron Garnets with Opposite Chirality. *ACS Photonics* **2016**, *3*, 1818–1825. [CrossRef]

40. Bi, L.; Hu, J.; Jiang, P.; Kim, H.S.; Kim, D.H.; Onbasli, M.C.; Dionne, G.F.; Ross, C.A. Magneto-Optical Thin Films for On-Chip Monolithic Integration of Non-Reciprocal Photonic Devices. *Materials* **2013**, *6*, 5094–5117. [CrossRef]

41. Bohnert, K.; Gabus, P.; Nehring, J.; Braendle, H.; Brunzel, M.G. Fiber-Optic Current Sensor for Electrowinning of Metals. *J. Lightw. Technol.* **1990**, *25*, 3544–3553. [CrossRef]

42. Huang, D.; Srinivasan, S.; Bowers, J.E. Compact Tb doped fiber optic current sensor with high sensitivity. *Opt. Express* **2015**, *23*, 247221. [CrossRef]

43. Andronova I.A.; Malykin, G.B. Physical problems of fiber gyroscopy based on Sagnac effect. *Phys.-Usp.* **2002**, *45*, 793–817. [CrossRef]

44. Chew, W.C. *Waves and Fields in Inhomogeneous Media*; Series on Electromagnetic Waves; IEEE Press: New York, NY, USA, 1995; Chapter 3, pp. 161–181, ISBN 0-7803-4749-8.

45. Snyder, A.W.; Sammut, R.A. Fundamental (HE_{11}) modes of graded optical fibers. *J. Opt. Soc. Am.* **1979**, *69*, 1663–1671. [CrossRef]

46. Fan, F.; Chen, S.; Chang, S.-J. A Review of Magneto-Optical Microstructure Devices at Terahertz Frequencies. *IEEE J. Sel. Top. Quantum Electron.* **2017**, *23*, 8500111. [CrossRef]

47. Firby C.J.; Elezzabi, A.Y. High-speed nonreciprocal magnetoplasmonic waveguide phase shifter. *Optica* **2015**, *2*, 598–606. [CrossRef]

48. Goell, J.E. A circular-harmonic computer analysis of rectangular dielectric waveguide. *Bell Syst. Tech. J.* **1969**, *48*, 2133–2160. [CrossRef]

49. Pollock, J.G.; Iyer, A.K.; Pratap, D.; Ramakrishna, S.A. A class of circular waveguiding structures containing cylindrically anisotropic metamaterials: Applications from radio frequency/microwave to optical frequencies. *J. Appl. Phys.* **2016**, *119*, 083103. [CrossRef]

50. Poladian, L.; Straton, M.; Docherty, A.; Argyros, A. Pure chiral optical fibres. *Opt. Express* **2011**, *19*, 968–980. [CrossRef] [PubMed]

51. Baltenkov, A.S.; Msezane, A.Z. Electronic quantum confinement in cylindrical potential well. *Eur. Phys. J. D* **2016**, *70*, 81. [CrossRef]